High Resolution Spectroscopic Measurements of Impurity Radiation Distributions and Neutral Deuterium Profiles in the JET Scrape-off Layer.

P Breger, R W T König, C F Maggi, Z A Pietrzyk*, D D R Summers, H P Summers, M G von Hellermann

JET Joint Undertaking, Abingdon,Oxon,OX143EA,United Kingdom

* CRPP Lausanne, Switzerland

1. Introduction

A periscope has been installed to image visible radiation from the plasma scrape-off layer at the top of JET on 49 fibres with 0.45cm spatial resolution. 44 fibres are imaged on the entrance slit of an astigmatism-corrected low- resolution spectrometer to yield a line integrated spatial emission profile, 5 fibres are passed to a high resolution spectrometer. Abel inversion of CIII and CVI line intensity profiles identifies emission layer positions. Passive charge-exchange radiation of CVI (n=8-7) is used to determine the fast neutral deuterium density in the edge.

2. Emission Layer Determination

Observed line intensity profiles are linked to local emissivity layers by a set of 44 coupled equations. For the Abel inversion the flux range ψ=0.5 to 1.2 is subdivided into 25 equidistant layers in ψ-space. The numerical inversion is obtained by a) a best fit solution for 25 emissivities and b) by a fit of two gaussian emission distributions. The average agreement between measured and simulated profile is ~15%.

The Doppler shift from the Li I emission of a 60 keV Li-beam yields accurate vertical position coordinates. The full EFIT equilibrium is used to provide a pathlength distribution along the viewing lines in flux space.

3. The Location of the Edge : CIII Emission Profiles

CIII profile measurements were taken on a sequence of pulses from an elm-free H-mode campaign with 5MA plasma current, 3 T field with new Be-tiles in the JET divertor. Both EFIT equilibrium and XLOC boundary determination give magnetic separatrix heights at major radius R=3.252m within ± 2cm. This position of the magnetic boundary agrees with thermal Li emission (vertical injection at R=3.252). The CIII intensity profile (λ=465.0nm) for two viewing mirror positions has a max. in channels intercepting the beam trajectory at height

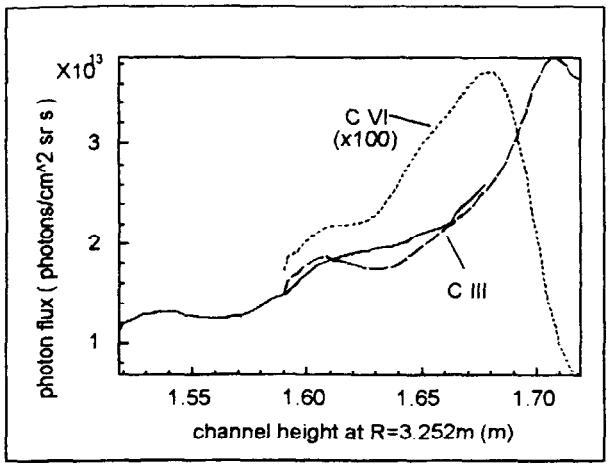

Fig. 1: Measured CIII intensity profile for two mirror positions. A CVI intensity profile is also shown.

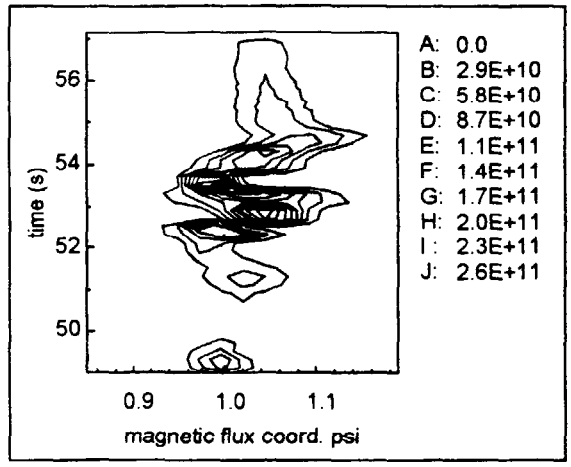

Fig. 2: Abel-inverted CIII emissivity distribution in photons/cm^3 sr s

1.7m (Fig.1), corresponding to the viewing line with maximum pathlength in the separatrix layer. Abel-inversion results for the CIII emission are shown in Figs.2-3. The position of the CIII emission layer is at ψ=1.0. The observed movement is correlated to errors in the magnetic data. During onset of the heating phase, the width of the CIII shell drops, and increases with the onset of giant elms, when the total shell emission also increases. At the end of the ICRH heating phase, the width of the shell decreases by factor 4 .

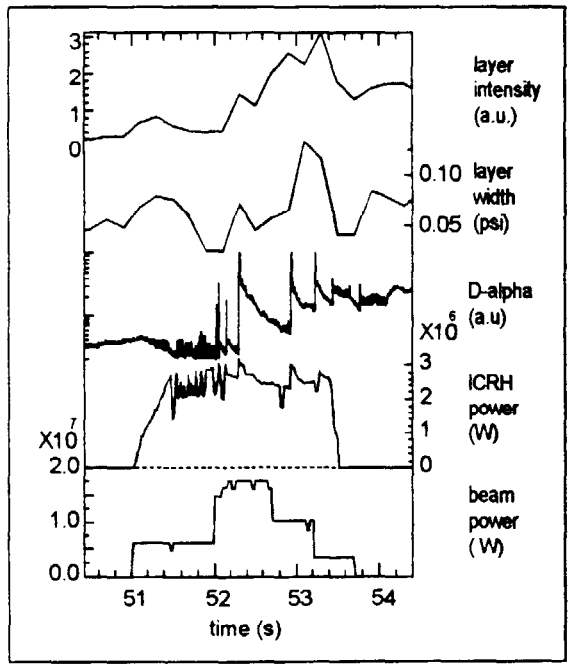

Fig.3: Time evolution of emission layer width and integrated layer intensity.

4. The "luke-warm" charge-exchange layer : CVI emission profiles

Plasma induced emission from CVI (λ=529.05nm) originates from two different emission layers : a "cold" feature (T_i~480 eV), corresponding to emission induced by electron collisions in the CVI ion shell, and a "luke-warm" feature (T_i~4keV) corresponding to cx-emission (see section 5). During high-performance hot-ion mode plasmas with 3.8 MA plasma current at 3.3T field, the passive cx feature is found by spectral line shape analysis to be 6 times more intense than the electron induced radiation. Because of errors in the magnetic data, the Abel inversion was done using an EFIT equilibrium shifted upwards by ~8.5cm (Figs. 4-5). The

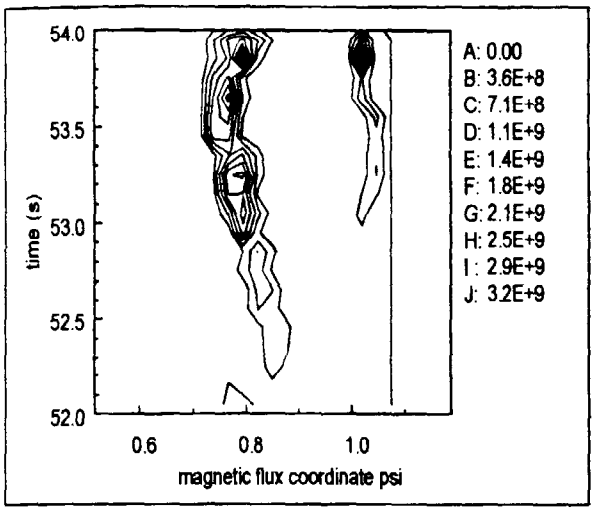

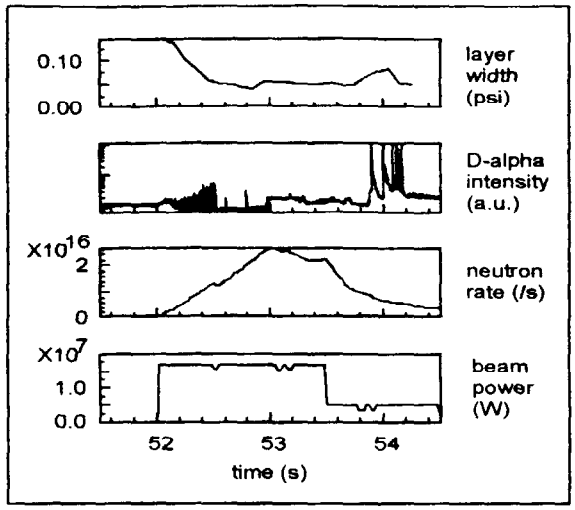

Fig.4: Emissivity distribution (photons/cm^{3}sr s)

Fig 5: Time evolution of cx-emission layer width

relative spacing of layers was found to be insensitive to vertical shifts. The outside emissivity layer is placed at the separatrix and is interpreted as the electron induced component. The layer at ψ~0.8 is attributed to the charge-exchange induced feature.The motion of the outer layer is seen to correlate exactly with the difference in magnetic prediction of plasma separatrix position at R=3.252m. This is also the case when comparing the motion of thermal Li-beam emission regions with that of the magnetic boundary. Comparing the width of the emission layer with the heating beam power and the vertical D_α-signal, a decrease during the development of the H-mode, and increase during the giant elm phase is seen (Fig. 5).

5. The fast Neutral Deuterium Distribution

Fast deuterons near the plasma edge region collide with cold recycling neutral deuterium. Resonant charge-exchange occurs with some of this recycling deuterium before it is ionised. The D population fraction in the n=2 level will charge-exchange resonantly with C^{6+} to give rise to the hot CVI (n=8) radiating shell :

$$\varepsilon_{CX}(R) = n_C^{6+}(R) \cdot n_D^{n=2}(R) \cdot Q_{eff}^{CX}(CVI, n = 8-7) \quad .$$

The effective emission coefficient Q has been calculated for the range of electron temperatures and densities as measured by LIDAR. Ion-temperature and C^{6+} concentration profiles are obtained from the heating-beam cx-diagnostics. The fast deuterium temperature is taken to be the same as the local plasma temperature inside the confined plasma, outside it has been fixed at 5 eV. For the inner cx-layer, electron excitation processes can be neglected as a source of N=8-7 radiation. Using a collisional radiative population model (ADAS) the total fast neutral

deuterium is estimated. A particular point of interest in this shot is the premature neutron rate roll-over at 53s, which is accompanied by increased levels of D_α emission. The integrated fast deuterium density rises by 25% during the roll-over at 53s, and another rise of 40% is seen during the power step-down at 53.5s.

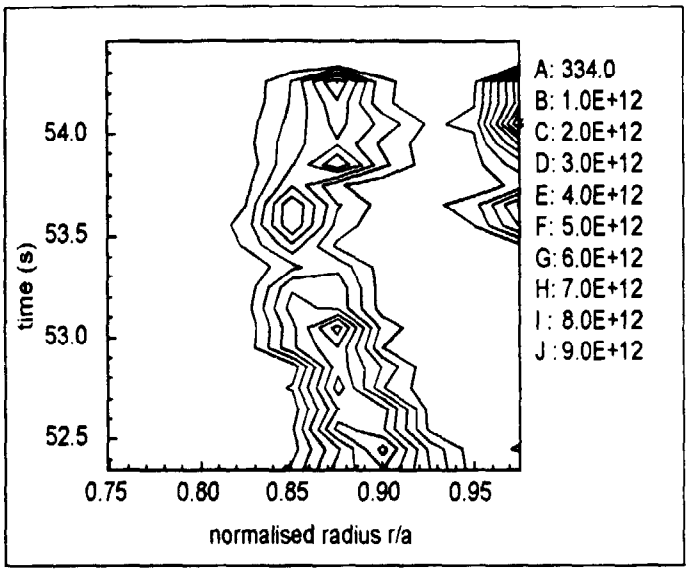

Fig. 6: Fast neutral deuterium density distribution in m^{-3}.

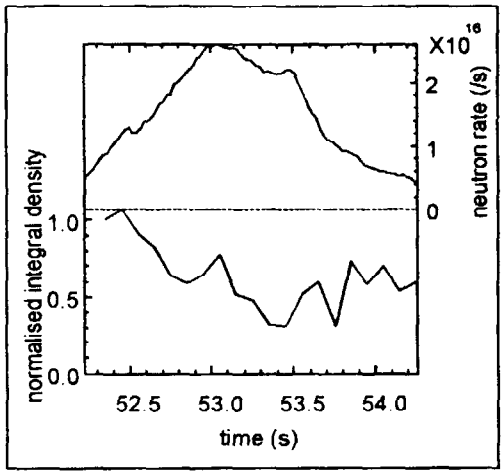

Fig. 7: Integrated deuterium density between r/a=0.8 and 0.94 compared to neutron rate

Although the neutral deuterium densities calculated at a depth of r/a=0.9 are rather small, the recycling cold deuterium which resonantly charge-exchanged with deuterons will have a much higher density, since the charge-exchange process has to compete with rapid ionisation.

7. Conclusions

- Passive intensity profiles may be used to identify the location plasma boundary location, and provide an independent means to verify positions from magnetic coil measurements.
- The existence of a hot charge-exchange induced layer interior to the plasma boundary was verified, and previous crude estimates of position and width could be substantiated.
- From the cx-emission layer a hot neutral deuterium density distribution could be calculated.
- Evidence for a neutral deuterium enhancement was found during the neutron rate roll-over phase.

We should like to thank the Swiss National Science Foundation for partially funding this work.